Journal of Solid Mechanics Vol. 12, No. 2 (2020) pp. 401-410
DOI: 10.22034/JSM.2019.1870009.1451

On Analysis of Stress Concentration in Curvilinear Anisotropic Deformable Continuum Bodies

Theddeus T. Akano [1,*], Omotayo A. Fakinlede [1], Patrick Shola Olayiwola [2]

[1] *Department of Systems Engineering, University of Lagos, Akoka, Lagos, Nigeria*
[2] *Department of Mechanical and Biomedical Engineering, Bells University of Technology Ota, Ogun, Nigeria*

Received 9 March 2020; accepted 9 May 2020

ABSTRACT

In cylindrical continua, hoop stresses are induced due to the circumferential failure. This mainly happens when the cylinder is subjected to mechanical loads that vary in the circumferential directions. On the other hand, radial stress is stress in the direction of or opposite to the central axis of a cylindrical body. In the present study, the influence of curvilinear anisotropy on the radial and tangential stresses of the polar-orthotropic hollow cylinder is presented. The governing equations were derived to evaluate the radial and hoop stresses inside the material. A semi-analytical method through differential transform method (DTM) for the polar-orthotropic hollow cylinder is implemented in the solution. The findings, based on polar-orthotropy, of the effect of the radial and circumferential loads on the radial and hoop stresses of the growing cylinders, show elastic responses that assist in identifying some of the outstanding properties of the curvilinear anisotropic continuums. It is also revealed that the characteristic response of various wall thicknesses of the cylindrical segment is influenced by the fibre orientation, radial and tangential stresses. This work has shown that the curvilinear anisotropy momentously affects the radial and hoop stresses on the polar-orthotropic hollow cylinder.

Keywords: Curvilinear anisotropy; Differential transform; Polar-orthotropy; Radial stress; Hoop stress.

1 INTRODUCTION

ANISOTROPY is the property of materials to exhibit variations in properties along various molecular axes [1]. This direction dependence affects the behaviour of the material. For instance, in fracture mechanics, the orientation of the microstructure of the material affects its stiffness and strength in various directions and consequently affects the direction of crack growth. Unlike isotropic materials that have material properties identical in all directions, anisotropic material's properties such as Young's Modulus, change with the direction along with the object. Common examples of anisotropic materials are wood and composites. Anisotropic materials have

*Corresponding author. Tel.: +23 48038496150.
E-mail address: takano@unilag.edu.ng (Theddeus T. Akano).

become relatively prevalent and more significant useful beginning since the recent part of the twentieth century. The rapid advancement influenced the need for new composite fibre materials for metal replacement in the aerospace systems. By this, composite materials were obtainable, in which the weight, stiffness, strength of the materials could be modelled around the anticipated application. This is the desired operational optimisation in the case of aircraft where it is favourite to orient an increased stiffness in the direction of the load, at the same time, sustaining a desirable strength to weight ratio. Anisotropic materials are either natural or human-made and are applied in several areas of study. Besides the magnetic anisotropy where the magnetic field is oriented in the desired direction, anisotropic heat conduction that is dependent on the geometry is another example of anisotropy application. Anisotropic materials are also a result of manufacturing processes like rolling or deep-drawing process can also result in the production of anisotropic materials. Composites transformed for definite applications.

Many engineering and biological materials have an anisotropic microstructure that would require a curvilinear anisotropic model. Natural examples may include wood with many cylindrical layers, tissues [2] and bones [3]. Many synthetic composite materials also exhibit such curvilinear microstructure. In consonant with rectilinear anisotropy, curvilinear anisotropy also occurs with some symmetries in material structure. When the material possesses a uniform cellular microstructure such that the properties have orthogonal symmetry with respect to the *r* and θ, it is classified as polar-orthotropic material (Fig. 1).

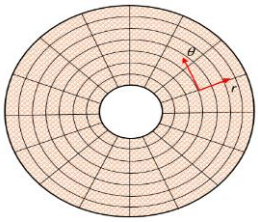

Fig.1
Polar-orthotropic material structure.

Major contributors in this field of study are few. Tarn [4], Galmudi and Dvorkin [5], and Horgan and Baxter [6] are very prominent in their contributions. The resulting partial differential equation is the solved by DTM that has successfully been applied to solve both linear and nonlinear systems of differential equations [7]–[17], and extended to biological equations [18]–[20].

The purpose of this work is to study the influence of material anisotropy and the thickness of a polar-orthotropic material structure on the radial and tangential stress concentrations on a curvilinear anisotropic body. This work will be limited to the two-dimensional case using a polar coordinate system model according to the curvilinear microstructure shown in Fig. 1. Here, the material is assumed to be of a cellular microstructure such that properties have orthogonal symmetry with respect to the *r* and *y* direction (Fig. 1). This assumption makes the material to be polar-orthotropic.

2 PROBLEM FORMULATION

The equations of equilibrium in polar coordinates could be expressed by applying a change of coordinates directly to the 2D Cartesian coordinate. However, it could be derived through the first principle by considering a material element that is being subjected to the three stresses $\sigma_{\theta\theta}$, σ_{rr} and $\sigma_{r\theta}$ (see Fig. 2). The dimensions of the element are dr in the radial direction, $rd\theta$ representing the inner surface, and $(r+dr)d\theta$ for the outer surface in the tangential direction.

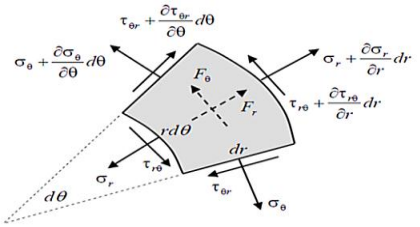

Fig.2
Two-dimensional differential element in polar coordinates.

The equilibrium of a two-dimensional differential element in polar coordinates is shown in Fig. 2. The two-dimensional equilibrium equations could explicitly be developed by the algebraic summation of the forces and moments. For the r coordinate, $\sum F_r = 0$, giving [5],

$$\left\{\begin{array}{l} F_r\, rdrd\theta + \left(\sigma_r + \dfrac{\partial \sigma_r}{\partial r}dr\right)(r+dr)d\theta + \left(\tau_{\theta r} + \dfrac{\partial \tau_{\theta r}}{\partial \theta}d\theta\right)dr\cos\left(d\theta/2\right) \\ -\left(\sigma_r\, rd\theta + \tau_{\theta r}dr\cos\left(d\theta/2\right) + \left(\sigma_\theta + \dfrac{\partial \sigma_\theta}{\partial \theta}d\theta\right)dr\sin\left(d\theta/2\right) + \sigma_\theta dr\sin\left(d\theta/2\right)\right) \end{array}\right\} = 0 \tag{1}$$

where the following expression could be derived:

$$\left.\frac{\sum F_r}{rdrd\theta}\right|_{dr,d\theta\to 0} = 0 = \frac{\partial \sigma_r}{\partial r} + \frac{1}{r}\frac{\partial \tau_{\theta r}}{\partial \theta} + \frac{\sigma_r - \sigma_\theta}{r} + F_r \tag{2}$$

Equally, for θ coordinate, $\sum F_\theta = 0$, giving,

$$\left\{\begin{array}{l} F_\theta\, rdrd\theta + \left(\tau_{r\theta} + \dfrac{\partial \tau_{r\theta}}{\partial r}dr\right)(r+dr)d\theta + \left(\tau_{\theta r} + \dfrac{\partial \tau_{\theta r}}{\partial \theta}d\theta\right)dr\sin\left(d\theta/2\right) \\ +\tau_{\theta r}dr\sin\left(d\theta/2\right) - \left(\tau_{r\theta}\, rd\theta + \left(\sigma_\theta + \dfrac{\partial \sigma_\theta}{\partial \theta}d\theta\right)dr\cos\left(d\theta/2\right) + \sigma_\theta dr\cos\left(d\theta/2\right)\right) \end{array}\right\} = 0 \tag{3}$$

where the following expression could be derived:

$$\left.\frac{\sum F_\theta}{rdrd\theta}\right|_{dr,d\theta\to 0} = 0 = \frac{\partial \tau_{r\theta}}{\partial r} + \frac{1}{r}\frac{\partial \sigma_\theta}{\partial \theta} + 2\frac{\tau_{\theta r}}{r} + F_\theta \tag{4}$$

The strain-displacement relations in general form is given as,

$$\mathbf{e} = \frac{1}{2}\left(\nabla\mathbf{u} + (\nabla\mathbf{u})^{\mathrm{T}}\right) \tag{5}$$

where $\mathbf{e}$ is the strain matrix and $\nabla\mathbf{u}$ is the displacement gradient matrix and $(\nabla\mathbf{u})^{\mathrm{T}}$ is its transpose. The strain, $\mathbf{e}$ is a symmetric (i.e. $e_{ij} = e_{ji}$) and is written as:

$$\mathbf{e} = \begin{bmatrix} e_{rr} & e_{r\theta} & e_{rz} \\ e_{r\theta} & e_{\theta\theta} & e_{\theta z} \\ e_{rz} & e_{\theta z} & e_{zz} \end{bmatrix} \tag{6}$$

The displacement, $\mathbf{u}$ in polar coordinates is written as, $\mathbf{u} = u_r\mathbf{e}_r + u_\theta\mathbf{e}_\theta + u_z\mathbf{e}_z$ with

$$\nabla\mathbf{u} = \left\{\begin{array}{l} \dfrac{\partial u_r}{\partial r}\mathbf{e}_r\mathbf{e}_r + \dfrac{\partial u_\theta}{\partial r}\mathbf{e}_r\mathbf{e}_\theta + \dfrac{\partial u_z}{\partial r}\mathbf{e}_r\mathbf{e}_z + \dfrac{1}{r}\left(\dfrac{\partial u_r}{\partial \theta} - u_\theta\right)\mathbf{e}_\theta\mathbf{e}_r + \dfrac{1}{r}\left(u_r + \dfrac{\partial u_\theta}{\partial \theta}\right)\mathbf{e}_\theta\mathbf{e}_\theta \\ +\dfrac{1}{r}\dfrac{\partial u_z}{\partial \theta}\mathbf{e}_\theta\mathbf{e}_z + \dfrac{\partial u_r}{\partial z}\mathbf{e}_z\mathbf{e}_r + \dfrac{\partial u_\theta}{\partial z}\mathbf{e}_z\mathbf{e}_\theta + \dfrac{\partial u_z}{\partial z}\mathbf{e}_z\mathbf{e}_z \end{array}\right\} \tag{7}$$

Giving the components of Eq. (7) as:

$$e_{rr}=\frac{\partial u_r}{\partial r};\quad e_{\theta\theta}=\frac{1}{r}\left(u_r+\frac{\partial u_\theta}{\partial \theta}\right);\quad e_{zz}=\frac{\partial u_z}{\partial z}$$
$$e_{r\theta}=\frac{1}{2}\left(\frac{1}{r}\frac{\partial u_r}{\partial \theta}+\frac{\partial u_\theta}{\partial r}-\frac{u_\theta}{r}\right);\quad e_{\theta z}=\frac{1}{2}\left(\frac{\partial u_\theta}{\partial z}+\frac{1}{r}\frac{\partial u_z}{\partial \theta}\right);\quad e_{zr}=\frac{1}{2}\left(\frac{\partial u_r}{\partial z}+\frac{\partial u_z}{\partial r}\right) \tag{8}$$

The constitutive law for the plane stress case could be written as:

$$\sigma_r=\frac{E_r}{1-\nu_{\theta r}\nu_{r\theta}}\left(e_r+\nu_{\theta r}e_\theta\right);\quad \sigma_\theta=\frac{E_\theta}{1-\nu_{\theta r}\nu_{r\theta}}\left(e_\theta+\nu_{r\theta}e_r\right) \tag{9}$$

Applying the strain-displacement equations, the Eq. (9) could be re-written as:

$$\sigma_r=\frac{E_r}{1-\nu_{\theta r}\nu_{r\theta}}\left(\frac{\partial u_r}{\partial r}+\nu_{\theta r}\frac{u_r}{r}\right);\quad \sigma_\theta=\frac{E_\theta}{1-\nu_{\theta r}\nu_{r\theta}}\left(\frac{u_r}{r}+\nu_{r\theta}\frac{\partial u_r}{\partial r}\right) \tag{10}$$

If axisymmetric is assumed, the stresses will be dependent on only the radial coordinate, making $\tau_{r\theta}=0$. As such, the equilibrium equation becomes,

$$\frac{\partial \sigma_r}{\partial r}+\frac{\sigma_r-\sigma_\theta}{r}+F_r=0 \tag{11}$$

Using the relation, $\nu_{\theta r}/E_\theta=\nu_{r\theta}/E_r$ and Eq. (10), Eq. (11) could be written as:

$$\frac{\partial^2 u_r}{\partial r^2}+\frac{1}{r}\frac{\partial u_r}{\partial r}-n^2\frac{1}{r^2}u_r+F_r=0 \tag{12}$$

where $n^2=E_\theta/E_r=\nu_{r\theta}/\nu_{\theta r}$ and n is an index for the measure of material anisotropy. When $n=1$, isotropy is recovered. For $n>1$, the material is circumferentially orthotropic [21], while for $n<1$ Horgan and Baxter [6] described the material as radially orthotropic.

3 APPLICATION OF DTM TO EQUILIBRIUM EQUATION

The present method is considered in the solution of Eq. (12). We will consider the situation when there is no radial force (i.e. $F_r=0$). The exact solution of the resulting equation is $u(r)=c_1r^n+c_2r^{-n}$, where c_1 and c_2 are constants which are unique to every boundary condition. Hence, the stresses could be expressed in this form:

$$\sigma_r=c_1r^{n-1}+c_2r^{-(n+1)};\quad \sigma_\theta=c_1n\,r^{n-1}-c_2n\,r^{-(n+1)} \tag{13}$$

Fig. 3 shows a thick-walled cylindrical boundary problem with both internal and external pressure loadings. The annular domain is defined with $b_1\le r\le b_2$ and the pressure loading, p will only be considered for b_2 (i.e. the outer boundary at $r=b_2$).

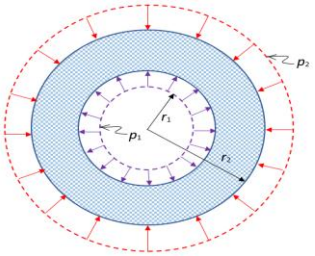

Fig.3
Thick-walled cylinder problem.

By applying the boundary conditions $\sigma_r(b_1)=0$ and $\sigma_r(b_2)=-p$, the stresses now become

$$\frac{\sigma_r}{p}=-\frac{b_2^{n+1}}{b_2^{2n}-b_1^{2n}}\left(r^{n-1}-b_1^{2n}r^{-(n+1)}\right);\quad \frac{\sigma_\theta}{p}=-\frac{nb_2^{n+1}}{b_2^{2n}-b_1^{2n}}\left(r^{n-1}+b_1^{2n}r^{-(n+1)}\right) \tag{14}$$

In order to overcome the difficulties encountered by the singularity at $x=0$, we use the transformation $t=\mathrm{In}(r)\Rightarrow r=e^t$. So that Eq. (12) becomes

$$\frac{\partial^2 u}{\partial t^2}-n^2u+F_r=0 \tag{15}$$

with various conditions. By employing the fundamental operations of DTM in Table 1., the following recurrence relation were obtained for Eq. (15):

$$U[k+2]=n^2\frac{\left(U(k)-F_r\delta(k)\right)}{(k+1)(k+2)} \tag{16}$$

For different conditions, the values of $U(k)$ could be evaluated from the recurrence relation. With the conditions $u(1)=0;u'(1)=1$, the transformed initial conditions become $u(t=0)=0;u'(t=0)=1$. The differential transform becomes $U(0)=0;U(1)=1$. We derived the remaining values of $U(k)$ from Eq. (16) as:

$$\begin{aligned}
&U(2)=-\frac{F_r n^2}{2}\\
&U(3)=\frac{n^2}{6}\\
&U(4)=-\frac{F_r n^4}{24}\\
&U(5)=\frac{n^4}{120}\\
&\vdots\\
&U(n)
\end{aligned} \tag{17}$$

Using Eq. (15), the closed form solution could be written as:

$$u(t)=t-\frac{1}{2}n^2F_rt^2+\frac{1}{6}n^2t^3-\frac{1}{24}n^4F_rt^4+\frac{1}{120}n^4t^5+\cdots \tag{18}$$

which upon making $F_r \to 0$, the exact solution becomes $u(r) = \frac{1}{2n}\left(r^n - r^{-n}\right)$ while Eq. (18) reduces to

$$u(t) = t + \frac{1}{6}n^2 t^3 + \frac{1}{120}n^4 t^5 + \frac{1}{5040}n^6 t^7 + \cdots \tag{19}$$

and after recalling that $t = \mathrm{In}(r)$, then,

$$u(r) = \mathrm{In}(r) + \frac{1}{6}n^2\left(\mathrm{In}(r)\right)^3 + \frac{1}{120}n^4\left(\mathrm{In}(r)\right)^5 + \frac{1}{5040}n^6\left(\mathrm{In}(r)\right)^7 + \cdots \tag{20}$$

Table 1
Comparison of the present method with exact solution for various *N* and *n* values.

r	*u(exact)*	*u(DTM)*	*% error*	*u(DTM)*	*% error*	*u(DTM)*	*% error*	*u(DTM)*	*% error*
		N=2, *n*=1		*N*=5, *n*=1		*N*=8, *n*=1		*N*=10, *n*=1	
2	0.75	0.748651	0.179828	0.75	$1.363*10^{-5}$	0.75	$5.94568*10^{-8}$	0.75	$1.82976*10^{-10}$
4	1.875	1.83033	2.38255	1.87495	0.00282846	1.875	$4.91608*10^{-5}$	1.875	$6.03704*10^{-7}$
6	2.91667	2.75047	5.69814	2.91613	0.018519	2.91665	0.000535817	2.91667	$1.09682*10^{-5}$
8	3.9375	3.57805	9.12883	3.93542	0.0529354	3.93742	0.00205663	3.9375	$5.65977*10^{-5}$
10	4.95	4.33726	12.3785	4.94474	0.106344	4.94975	0.00505236	4.94999	0.0001702
		N=8, *n*=2		*N*=10, *n*=2		*N*=12, *n*=2		*N*=15, *n*=2	
2	0.9375	0.9375	$4.91608*10^{-5}$	0.9375	$6.03704*10^{-7}$	0.9375	$5.51323*10^{-9}$	0.9375	$2.25862*10^{-13}$
4	3.98438	3.9834	0.0245953	3.98433	0.00119646	3.98437	$4.34279*10^{-5}$	3.98437	$2.73109*10^{-8}$
6	8.99306	8.97601	0.189576	8.99168	0.015269	8.99297	0.000920451	8.99306	$1.60423*10^{-6}$
8	15.9961	15.9057	0.564939	15.9864	0.0608069	15.9953	0.00491188	15.9961	$1.54365*10^{-5}$
10	24.9975	24.7127	1.13927	24.9602	0.149302	24.9938	0.0147201	24.9975	$6.91746*10^{-5}$
		N=10, *n*=3		*N*=15, *n*=3		*N*=18, *n*=3		*N*=20, *n*=3	
2	1.3125	1.3125	$5.65977*10^{-5}$	1.3125	$2.31834*10^{-10}$	1.3125	$2.39145*10^{-12}$	1.3125	$2.92541*10^{-14}$
4	10.6641	10.6576	0.0608069	10.6641	$1.5437*10^{-5}$	10.6641	$6.31167*10^{-7}$	10.6641	$2.14573*10^{-8}$
6	35.9992	35.8061	0.536471	35.999	0.00061614	35.9992	0.000041875	35.9992	$2.36913*10^{-6}$
8	85.333	83.9234	1.65194	85.3292	0.00451294	85.3327	0.00041129	85.333	$3.12364*10^{-5}$
10	166.667	161.108	3.33485	166.639	0.0163901	166.663	0.00182423	166.666	0.000169365
		N=1, *n*=0.1		*N*=2, *n*=0.1		*N*=3, *n*=0.1		*N*=4, *n*=0.1	
2	0.693702	0.693702	$1.92231*10^{-5}$	0.693702	$1.9223*10^{-5}$	0.693702	$2.19888*10^{-9}$	0.693702	$2.19888*10^{-9}$
4	1.39074	1.39073	0.000306937	1.39073	0.00030694	1.39074	$1.4042*10^{-7}$	1.39074	$1.4042*10^{-7}$
6	1.80136	1.80135	0.000854965	1.80135	0.00085497	1.80136	$6.53311*10^{-7}$	1.80136	$6.53311*10^{-7}$
8	2.09446	2.09443	0.00154856	2.09443	0.00154856	2.09446	$1.59362*10^{-6}$	2.09446	$1.59362*10^{-6}$
10	2.32299	2.32293	0.00232487	2.32293	0.00232487	2.32299	$2.93327*10^{-6}$	2.32299	$2.93327*10^{-6}$
		N=1, *n*=0.5		*N*=2, *n*=0.5		*N*=4, *n*=0.5		*N*=5, *n*=0.5	
2	0.707107	0.707023	0.0118191	0.707023	0.0118191	0.707107	$3.37604*10^{-5}$	0.707107	$5.6288*10^{-8}$
4	1.5	1.4973	0.179828	1.4973	0.179828	1.49997	0.00204733	1.5	$1.36302*10^{-5}$
6	2.04124	2.03144	0.480303	2.03144	0.480303	2.04106	0.00910547	2.04124	0.00010111
8	2.47487	2.45409	0.839617	2.45409	0.839617	2.47434	0.0213796	2.47487	0.000319331
10	2.84605	2.81125	1.22258	2.81125	1.22258	2.84497	0.038078	2.84603	0.000696533

4 RESULTS AND DISCUSSIONS

Attempts on limiting analysis for the anisotropic case (i.e. $n \neq 1$) have proved abortive with non-converged solution [5]. This amazing effect is linked to the fact that the stresses will become unbounded when $n < 1$, as $b_2 \to \infty$. For this problem, the internal radius of a thick cylinder is chosen such that the radial stress at its inner boundary is tuned to zero, i.e. $\sigma_r(b_1) = 0$. At the outer boundary coinciding with the external radius, however, the radial stress $\sigma_r(b_2) = -p$, the external pressure that is everywhere compressive on the annular domain. On the other hand, the tangential (hoop) stresses, $\sigma_\theta(b_1)$ and $\sigma_\theta(b_2)$ become everywhere tensile.

Figs. 4-7 show the dimensionless distribution plots of radial and hoop stresses for various values of *n* (i.e. $n = 0.4, 0.7, 1.0, 1.3, 1.6$) when $b_2/b_1 = 6.5$ and $b_2/b_1 = 2.5$. For values of $n > 1$, the magnitude of the radial stress

is less than that of the isotropic. This type of anomaly is referred to as refer stress shielding [5]. However, the reverse is noticed for values of $n<1$, where the isotropic stress magnitude is less than that of the radial, thus causing stress amplification. These two effects can be regarded as being correlated to the decay of boundary conditions. It could also be observed that the hoop stress magnitude at $r=b_1$ decreases as the values of n increases. It could be inferred that; the curvilinear anisotropy momentously affects the radial and hoop stresses.

Fig. 4 illustrates the family of curves for the radial stress distribution against the radius within the annular domain of the thick cylinder. It is shown that before the critical point (which is about 6.5 times the value of internal radius), and for different values of index n, increasing the radius of annular domain causes increase in the value of radial stress, but after this focal point, further increase in the domain radius results in decrease of the radial stress.

In Fig. 5, the shown family of hyperbolas depicted the relationship between the tangential (hoop) stress distribution and the annular domain radius for various values of n. It is notable that increasing the radius causes a decrease in the value of tangential stress; however, after the critical value of about 3.5 times the internal radius of the cylinder, further increase of the radius gives increase in the value of the tangential stress.

The family of curves shown in Fig. 6 demonstrates the radial stress distribution against the ratio of the external-to-internal radius of the annular domain of the cylinder. The critical value is where b_2/b_1 is about 4.5. When $n>1$, further increase in the value of b_2/b_1 results in decline of the value of radial stress, which is everywhere compressive. With $n<1$, increasing the value of b_2/b_1, causes increase in the radial stress value. At the point when $n=1$, equal value of stress is maintained with further increase in b_2/b_1.

The hoop stress distribution profile of Fig. 7 is similar to that of Fig. 6, except that while tangential stress distribution is everywhere tensile, the latter is everywhere compressive.

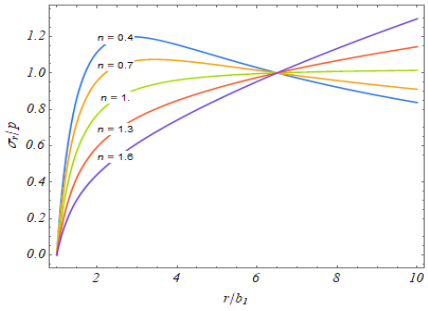

Fig.4
Radial stress distributions for different values of n in a polar orthotropic annular domain, $b_1 \le r \le b_2$ and pressure loading, p for $b_2/b_1 = 6.5$.

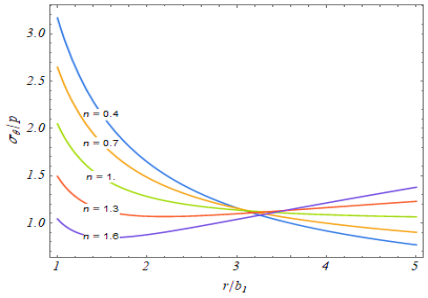

Fig.5
Hoop stress distributions for different values of n in a polar orthotropic annular domain, $b_1 \le r \le b_2$ and pressure loading, p for $b_2/b_1 = 6.5$.

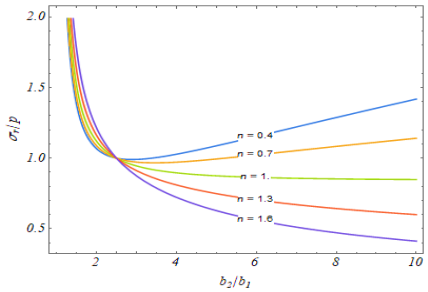

Fig.6
Radial stress distributions for different values of n in a polar orthotropic annular domain, $b_1 \le r \le b_2$ and pressure loading, p for $r/b_1 = 2.5$.

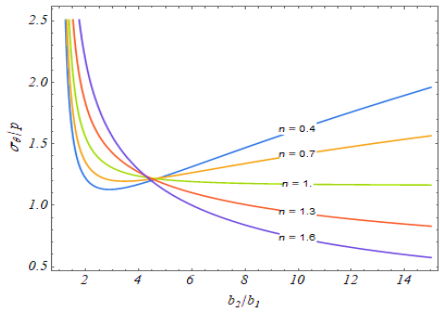

Fig.7
Hoop stress distributions for different values of n in a polar orthotropic annular domain, $b_1 \le r \le b_2$ and pressure loading, p for $r/b_1 = 2.5$.

As described by Figs. 8-10, the radial stress distribution profiles are families of parabolas that illustrate stress against the radius r/b_1 . It is observed that when $n < 1$, increasing the ratio gives rise to sharp increase in the value of radial stress to maximum points, then start to decline (Fig. 8), but when $n = 1$, increasing the radius results in initially increasing the radial stress value and after the peaks, indifference is recorded for further increase in radius of the annular domain (Fig. 9), however with $n > 1$, increase of the radius gives parabolic increase in the stress value (Fig. 10).

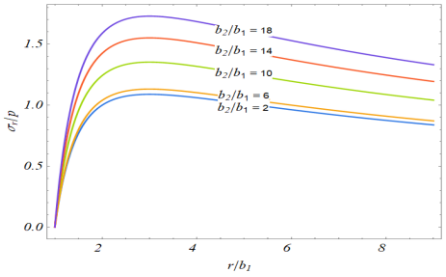

Fig.8
Radial stress distributions for different values of b_2/b_1 in a polar orthotropic annular domain, $b_1 \le r \le b_2$ and pressure loading, p for $n < 1$.

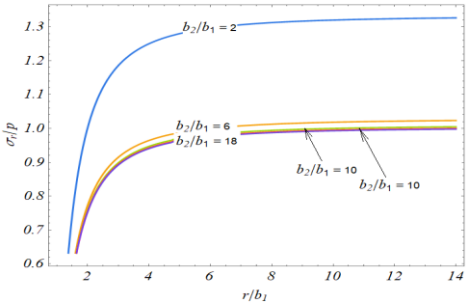

Fig.9
Radial stress distributions for different values of b_2/b_1 in a polar orthotropic annular domain, $b_1 \le r \le b_2$ and pressure loading, p for $n = 1$.

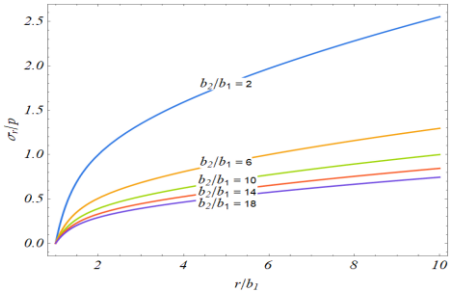

Fig.10
Radial stress distributions for different values of b_2/b_1 in a polar orthotropic annular domain, $b_1 \le r \le b_2$ and pressure loading, p for $n > 1$.

Hoop stress distributions for various values of b_2/b_1 against the annular domain radius, r/b_1 , are illustrated by Figs. 11 through 13. The families of hyperbolic curves for the case $n < 1$ in Fig. 11 showed that the tangential

(hoop) stress increase with increasing ratio b_2/b_1, but decrease with increasing values of the radius of the polar orthotropic annular domain. For the case $n=1$, decreasing the values of the ratio b_2/b_1 increases the values of the hoop stress, but decreases it when the annular radius is increasing (Fig. 12). With $n>1$, Fig. 13 showed that the value of hoop stress increases with decreasing values of the ratio b_2/b_1 but initially decreases sharply as the domain radius r/b_1 increases and makes a turning point at about $r/b_1>1.5$ to increase as the domain radius further increases.

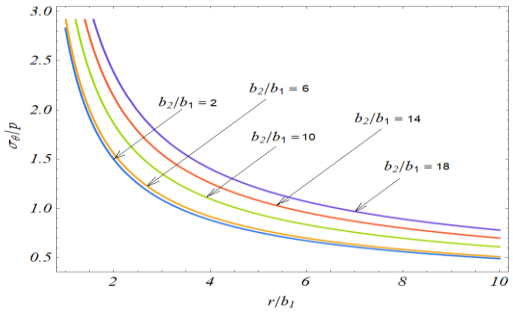

Fig.11
Hoop stress distributions for different values of b_2/b_1 in a polar orthotropic annular domain, $b_1 \le r \le b_2$ and pressure loading, p for $n<1$.

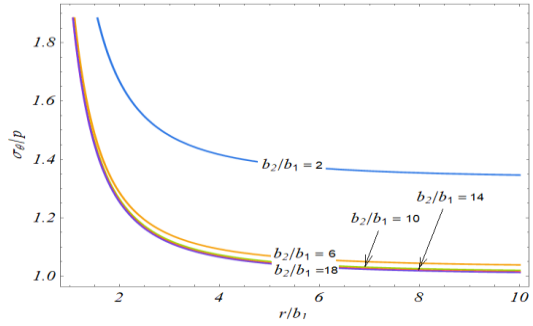

Fig.12
Hoop stress distributions for different values of b_2/b_1 in a polar orthotropic annular domain, $b_1 \le r \le b_2$ and pressure loading, p for $n=1$.

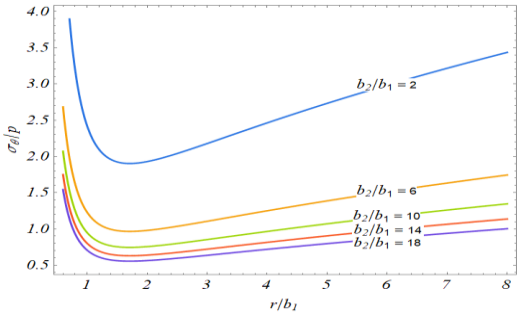

Fig.13
Hoop stress distributions for different values of b_2/b_1 in a polar orthotropic annular domain, $b_1 \le r \le b_2$ and pressure loading, p for $n>1$.

5 CONCLUSION

The stress analysis in cylindrical segments has been studied. The analysis shows that the characteristic response of various wall thicknesses of the cylindrical segment is influenced by the fibre orientation, radial and tangential stresses. The measure of material anisotropy, n is another critical factor which greatly affects the curvilinear deformation of the fibre segments. The radial stress varies around the critical point at different values of n. Similarly, the tangential stress increases proportionately with the radius until the critical point is attained. The tangential stress tends to decrease again after the critical point showing that the curvilinear anisotropy significantly affects both the radial and tangential stresses on the polar-orthotropic hollow cylinder. Also, the differential transform method has been proven to be a viable approach towards the solution of problems in curvilinear anisotropy.

REFERENCES

[1] Newnham R.E., 2005, *Properties of Materials : Anisotropy, Symmetry, Structure*, Oxford University Press.

[2] Humphrey J.D., 2003, Continuum biomechanics of soft biological tissues, *Proceedings of the Royal Society A: Mathematical, Physical and Engineering Sciences* **459**(2029): 3-46.

[3] Wang L., Song J., Ortiz C., Boyce M.C., 2009, Anisotropic design of a multilayered biological exoskeleton, *Journal of Materials Research* **24**(12): 3477-3494.

[4] Tarn J.-Q., 2001, Exact solutions for functionally graded anisotropic cylinders subjected to thermal and mechanical loads, *International Journal of Solids and Structures* **38**(46–47): 8189-8206.

[5] Gal D., Dvorkin J., 1995, Stresses in anisotropic cylinders, *Mechanics Research Communications* **2**(2):109-113.

[6] Horgan C.O., Baxter S.C., 1996, Effects of curvilinear anisotropy on radially symmetric stresses in anisotropic linearly elastic solids, *Journal of Elasticity* **42**(1): 31-48.

[7] Zhou J.K., 1986, *Differential Transformation and its Applications for Electrical Circuits*, Huazhong University Press, Wuhan, China.

[8] Ayaz F., 2004, Solutions of the system of differential equations by differential transform method, *Applied Mathematics and Computation* **147**(2): 547-567.

[9] Arikoglu A., Ozkol I., 2006, Solution of differential-difference equations by using differential transform method, *Applied Mathematics and Computation* **181**(1): 153-162.

[10] Liu H., Song Y., 2007, Differential transform method applied to high index differential–algebraic equations, *Applied Mathematics and Computation* **184**(2): 748-753.

[11] Rashidifar M.A., Rashidifar A.A., 2013, Analysis of vibration of a pipeline supported on elastic soil using differential transform method, *American Journal of Mechanical Engineering* **1**(4): 96-102.

[12] Mohamed M.A., 2010, Comparison differential transformation technique with adomian decomposition method for dispersive long-wave equations in (2+ 1)-dimensions, *Applications and Applied Mathematics* **5**(1): 148-166.

[13] Jena S.K., Chakraverty S., 2019, Differential quadrature and differential transformation methods in buckling analysis of nanobeams, *Curved and Layered Structures* **6**(1): 68-76.

[14] Shali S., Nagaraja S.R., Jafarali P., 2017,Vibration of non-uniform rod using Differential Transform Method, *IOP Conference Series: Materials Science and Engineering* **225**(1): 12027.

[15] Kumar M., Reddy G.J., Kumar N.N., Bég O.A., 2019, Application of differential transform method to unsteady free convective heat transfer of a couple stress fluid over a stretching sheet, *Heat Transfer Research* **48**(2): 582-600.

[16] Biazar J., Eslami M., 2011, Differential transform method for nonlinear fractional gas dynamics equation, *International Journal of Physical Sciences* **6**(5): 1203-1206.

[17] Shit G.C., Mukherjee S., 2019, Differential transform method for unsteady magnetohydrodynamic nanofluid flow in the presence of thermal radiation, *Journal of Nanofluids* **8**(5): 998-1009.

[18] Tari A., 2012, The differential transform method for solving the model describing biological species living together, *Iranian Journal of Mathematical Sciences and Informatics* **7**(2): 63-74.

[19] Gökdoğan A., Merdan M., Yildirim A., 2012, The modified algorithm for the differential transform method to solution of Genesio systems, *Communications in Nonlinear Science and Numerical Simulation* **17**(1): 45-51.

[20] Benhammouda B., Vazquez-Leal H., Hernandez-Martinez L., 2014, Modified differential transform method for solving the model of pollution for a system of lakes, *Discrete Dynamics in Nature and Society* **2014**: 645726.

[21] Vasilenko A.T., Sudavtsova G.K., 2001, Elastic equilibrium of circumferentially inhomogeneous orthotropic cylindrical shells of arbitrary thickness, *International Applied Mechanics* **37**(8): 1046-1054.